RESEARCH ARTICLE

Check for updates

Core−shell heterojunction engineering of Co₃O₄/NiFe LDH nanosheets as bifunctional electrocatalysts for efficient reduction of nitrite to ammonia†

Yi Feng,[a] Jin-Tao Ren,[a] Hao-Yu Wang,[a] Lei Wang[a] and Zhong-Yong Yuan ⓘ *[a,b]

An electrocatalytic NO_2^- reduction reaction (NO_2^-RR) has cast new light on renewable NH_3 synthesis and treatment of NO_2^--contaminated aquatic ecosystems. Numerous studies have been devoted to developing NO_2^-RR electrocatalysts with superior selectivity. However, few efforts have focused on constructing bifunctional catalysts promoting the NO_2^-RR and the oxygen evolution reaction (OER) simultaneously, which is significant to reduce the energy consumption and cost of electrocatalytic ammonia production. Herein, we demonstrate the core−shell heterostructures of NiFe LDH nanoarrays attached to Co_3O_4 nanosheets on Ni foam, which exhibit an excellent NO_2^-RR performance (yield: 4.27 mg h^{-1} cm^{-2}, FE: 96.53% at −0.5 V) and a remarkable OER performance (η_{100}: 270 mV) as well as decent stability. Furthermore, a two-electrode electrolyzer assembled with Co_3O_4/NiFe LDH heterostructures only requires 1.55 V to reach 10 mA cm^{-2}, approaching that of the ammonia production system assembled with a noble-metal-based catalyst. The decent NO_2^-RR and OER properties benefit from the optimized electronic structure due to the heterojunction formation and the increased electrochemically active area owing to the core−shell structure construction. This effort offers new insights into achieving high-efficiency and low-cost electrocatalytic ammonia production.

1. Introduction

NH_3 is one of the most essential industrial raw materials for synthesizing substantially all nitrogen-based fertilizers, accounting for 5% of the chemical market value.[1–3] Recently, NH_3 has also been acknowledged as an intriguing carbon-free energy carrier due to the merits of competitive delivery cost, large hydrogen capacity, and excellent energy density.[4] However, with the unceasing employment of the industrial Haber–Bosch route for NH_3 production characterized by high energy consumption and large carbon dioxide emission, the global energy crisis will inevitably be aggravated and the achievement of carbon neutrality will be hindered.[5] Consequently, it is highly imperative to explore alternative routes for sustainable ammonia production.

Among these alternative routes, electrocatalytic reduction of nitrogenous species under ambient conditions has emerged as

an attractive approach on account of its appealing cost and environmental friendliness.[1] In contrast to the extensively studied electrochemical N_2 reduction system with bleak performance, the electrocatalytic NO_2^- reduction reaction (NO_2^-RR) has cast new light on renewable NH_3 synthesis as NO_2^- exhibits substantially increased solubility in water and lower cleavage energy than N_2.[2–4] In addition, NO_2^- represents one of the severest contaminants of the aquatic ecosystem owing to its poisonous nature and high concentration, potentially jeopardizing public health and disrupting the nitrogen cycle. Apparently, electrocatalytic NO_2^- reduction can also contribute to the treatment of NO_2^--contaminated aquatic ecosystems, thus restoring the damage caused by the disturbed nitrogen cycle.[5] However, the reaction kinetics of the NO_2^-RR remains intractable due to the sophistication of the $6e^-$ process.[6] Moreover, the NO_2^-RR faces the challenge of competing with other side reactions under aqueous conditions including the hydrogen evolution reaction (HER). In the aqueous catalytic installations currently employed for ammonia production, the anode reaction coupled with the NO_2^-RR is the oxygen evolution reaction (OER). The OER also faces challenges regarding sluggish kinetics due to its four-electron transfer.[7–9] Consequently, the exploration of NO_2^-RR and OER bifunctional catalysts characterized by improved overpotential and superior selectivity contributes to simplifying the require-

[a]*National Institute for Advanced Materials, School of Materials Science and Engineering, Smart Sensing Interdisciplinary Science Center, Nankai University, Tianjin 300350, China. E-mail: zyyuan@nankai.edu.cn*

[b]*Key Laboratory of Advanced Energy Materials Chemistry (Ministry of Education), Nankai University, Tianjin 300071, China*

†Electronic supplementary information (ESI) available. See DOI: https://doi.org/10.1039/d3qi00795b

4510 | *Inorg. Chem. Front.*, 2023, **10**, 4510–4518

This journal is © the Partner Organisations 2023

ments for equipment and electrode preparation techniques, leading to electrocatalytic ammonia production with competitive cost and lower energy consumption.[10,11] Nevertheless, few efforts are currently made on exploring highly selective and active NO_2^-RR and OER bifunctional catalysts.

Co_3O_4 has been broadly studied for electrocatalytic conversion of nitrogen-oxyanions (NO_x^-) into NH_3 due to the decent intrinsic electrocatalytic activity.[12] However, the actual ammonia production performance of Co_3O_4 still falls short of expectations owing to the inferior electrical conductivity caused by the large intrinsic band gap. Various strategies have been employed to improve Co_3O_4 performance, such as introducing vacancies,[13] heteroatom doping[14] and constructing heterojunctions.[12] The obtained Co_3O_4-based materials exhibit favourable NH_3 yields and superior Faraday efficiencies; nevertheless, the availability of Co_3O_4-based materials as NO_2^-RR and OER bifunctional catalysts is restricted by the poor inherent OER activity of Co_3O_4.[15] Recently, tremendous interest has been dedicated to interfacial engineering of excellent core–shell structures by coupling two components,[16–18] which is conducive to achieving enhanced electrocatalytic activity and better integration of the advantages of each component, by accelerating electron transfer, decreasing the ion diffusion distance and creating strong coupling effects between different components. For example, a core–shell heterostructured composite is formed by coupling MoS_2, possessing remarkable HER activity, and NiFe LDH, characterized by promising OER activity, requiring only 1.61 V for achieving 10 mA cm^{-2} in overall water splitting.[19] The decent HER and OER bifunctional properties of the material are mainly derived from two aspects: (1) the optimized electron configuration and regulated adsorption/desorption energy on account of heterogeneous structures; (2) the enlarged contact surface between the electrode and electrolyte caused by the formation of core–shell structures. Considering the promising feasibility of core–shell interfacial engineering[20] and the prominent OER performance of NiFe LDH,[21,22] obtaining remarkable NO_2^-RR and OER bifunctional electrocatalysts is extremely promising through the construction of core–shell Co_3O_4/NiFe LDH heterostructures.

Herein, we report core–shell Co_3O_4/NiFe LDH heterostructured nanosheets with NiFe LDH nanoarrays attached to Co_3O_4 nanosheets, which serve as efficient and robust NO_2^-RR and OER bifunctional catalysts. To further enhance the electrical conductivity and structural toughness of the electrocatalyst, Co_3O_4/NiFe LDH nanoarrays are grown directly on Ni foam. The combination with NiFe LDH not only introduces OER active sites but also optimizes the charge distribution of NO_2^-RR active sites on Co_3O_4. Furthermore, the construction of the optimized core–shell structure is achieved after regulating the time of growing NiFe LDH, increasing the contact area between the electrolyte and catalyst and creating more abundant electrolyte permeation channels. The optimized Co_3O_4/NiFe LDH nanosheets demonstrate an excellent NO_2^-RR performance (yield: 4.27 mg h^{-1} cm^{-2}, FE: 96.53% at −0.5 V) and a remarkable OER performance (η_{100}: 270 mV) as well as decent stability. And a two-electrode cathode–anode coupled

ammonia production system assembled with Co_3O_4/NiFe LDH heterostructures only requires 1.55 V to reach 10 mA cm^{-2}, approaching that of the system assembled with precious metal-based materials.

2. Experimental section

2.1. Synthesis of electrocatalysts

The heterostructured Co_3O_4/NiFe LDH nanoarrays were obtained by an electrodeposition–calcination–electrodeposition process on nickel foam. The first electrodeposition was conducted in a three-electrode system by employing clean nickel foam (2.5 × 2.5 cm), a Pt electrode, and a mercury oxide electrode as the working, counter, and reference electrode, respectively. The first electrolyte is a reddish solution (0.05 M $Co(NO_3)_2 \cdot 6H_2O$) used for the electrochemical preparation of $Co(OH)_2$/NF. The relevant conditions were adjusted to potential reaching −1.0 V vs. Hg/HgO for 10 min. Then, Co_3O_4/NF was obtained by calcining $Co(OH)_2$/NF after fully drying at 350 °C under a N_2 atmosphere for 2 h. In order to obtain Co_3O_4/NiFe LDH, the second electrodeposition was performed on Co_3O_4/NF. The conditions in the second electrodeposition of NiFe LDH are similar to those of the first, apart from the electrolyte (0.15 M $Ni(NO_3)_2 \cdot 6H_2O$ + 0.15 M $FeSO_4 \cdot 7H_2O$) and deposition duration. By adjusting the deposition duration (20, 40, and 60 s), a series of catalysts (Co_3O_4/NiFe LDH-x, x represents the number of seconds used for the growth of NiFe LDH) were obtained. In the series of catalysts, Co_3O_4/NiFe LDH-40 shows the best NO_2^-RR and OER bifunctional performance. For comparison, pure NiFe LDH/NF can also be grown on NF via the same electrodeposition approach.

2.2. Characterization

The chemical compositions of the materials were analyzed by X-ray powder diffraction (XRD, Rigaku Smart Lab, with Cu Kα radiation) and X-ray photoelectron spectroscopy (XPS, PHI 5000). The morphologies of materials were analyzed by scanning electron microscopy (FE-SEM, Jeol JSM-7800) and transmission electron microscopy (TEM, Jeol JEM-2800).

2.3. Electrochemical measurement

The NO_2^-RR performances were measured in a classic H-type cell with Nafion 117 membrane separation, employing the synthesized catalysts (1 × 1 cm^2) as the working electrode with a WaveDrive 20 Bipotentiostat/Galvanostat (Pine Research Instrumentation, USA). A Pt wire and Ag/AgCl electrode were employed as the counter and reference electrodes. 35–40 mL Ar-saturated electrolyte solutions (0.1 M NaOH with and without 0.1 M NO_2^-) were added to two cells of the H-type electrolyzer. The OER performance was evaluated using a traditional three-electrode system with an electrolyte (1 M KOH), a reference electrode (Ag/AgCl electrode) and a counter electrode (graphitic rod). The electrocatalytic ammonia production was carried out in a two-electrode system. All voltages used in our effort were transformed into the potential of the reversible

This journal is © the Partner Organisations 2023

Inorg. Chem. Front., 2023, **10**, 4510–4518 | **4511**

hydrogen electrode (RHE) using the equation:

$$E_{RHE} = E_{Ag/AgCl} + 0.197\ V + 0.059\ V \times pH.$$

3. Results and discussion

3.1 Materials synthesis and characterization

The fabrication process of Co_3O_4/NiFe LDH supported on Ni foam is depicted in Fig. 1a. First, Co_3O_4/NF was obtained by an electrodeposition–calcination process. Co_3O_4 nanosheets were grown vertically on nickel foam (Fig. 1b). Then Co_3O_4/ NiFe LDH was obtained by subsequent electrodeposition on Co_3O_4/NF. NiFe LDH/NF can also be obtained by a similar electrodeposition on Ni foam. The SEM image of NiFe LDH/NF (Fig. 1c) shows staggered NiFe LDH nanosheets with smaller dimensions uniformly distributed on the Ni foam. Obviously, the deposition duration of NiFe LDH on Co_3O_4/NF is critical for constructing core–shell Co_3O_4/NiFe LDH heterostructures and obtaining a prominent active surface area. After the optimum electrodeposition of NiFe LDH on Co_3O_4/NF, Co_3O_4/ NiFe LDH-40 exhibited a core–shell structure, clearly depicted in Fig. 1d, which is based on Co_3O_4 nanosheets with larger dimensions as cores and interlaced NiFe LDH nanoarrays as shells. Such a core–shell structure is extremely conducive to increasing the electrochemically active reaction area and constructing more abundant electrolyte permeation channels, thus exposing more active sites and accelerating mass transfer.[23–25] Excessively long and short electrodeposition times were also probed for their effects on the construction of core–shell Co_3O_4/NiFe LDH heterostructures. A short time led to insufficient exposure of active sites (Fig. S1a†), while an overly long time induced agglomeration of NiFe LDH on the surface, resulting in the blockage of active sites and slower mass transport (Fig. S1b†).

The X-ray diffraction (XRD) pattern (Fig. 1e) was employed for probing the crystal structure of the optimal Co_3O_4/NiFe LDH-40 sample. In Fig. 1e, the diffraction peaks positioned at around $2\theta = 36.9°$, $94.1°$ and $99.3°$ can correspond to the (311), (731) and (800) crystallographic planes of Co_3O_4 (PDF # 42-1467),[26] respectively. Other diffraction peaks at the vicinity of $2\theta = 31.3°$ and $65.1°$ can be well indexed to the (101) and (116) characteristic crystalline planes belonging to NiFe LDH (PDF # 40-0215).[27] Sufficient evidence is provided in Fig. 1e to verify that Co_3O_4/NiFe LDH-40 is successfully synthesized. The detailed structure of the optimized Co_3O_4/NiFe LDH-40 sample was further investigated employing a transmission electron microscope (TEM). The shell made of interlaced nanosheets of Co_3O_4/NiFe LDH-40 is reconfirmed in Fig. 1f. Two lattice fringe spacings of 0.243 and 0.143 nm are displayed on the

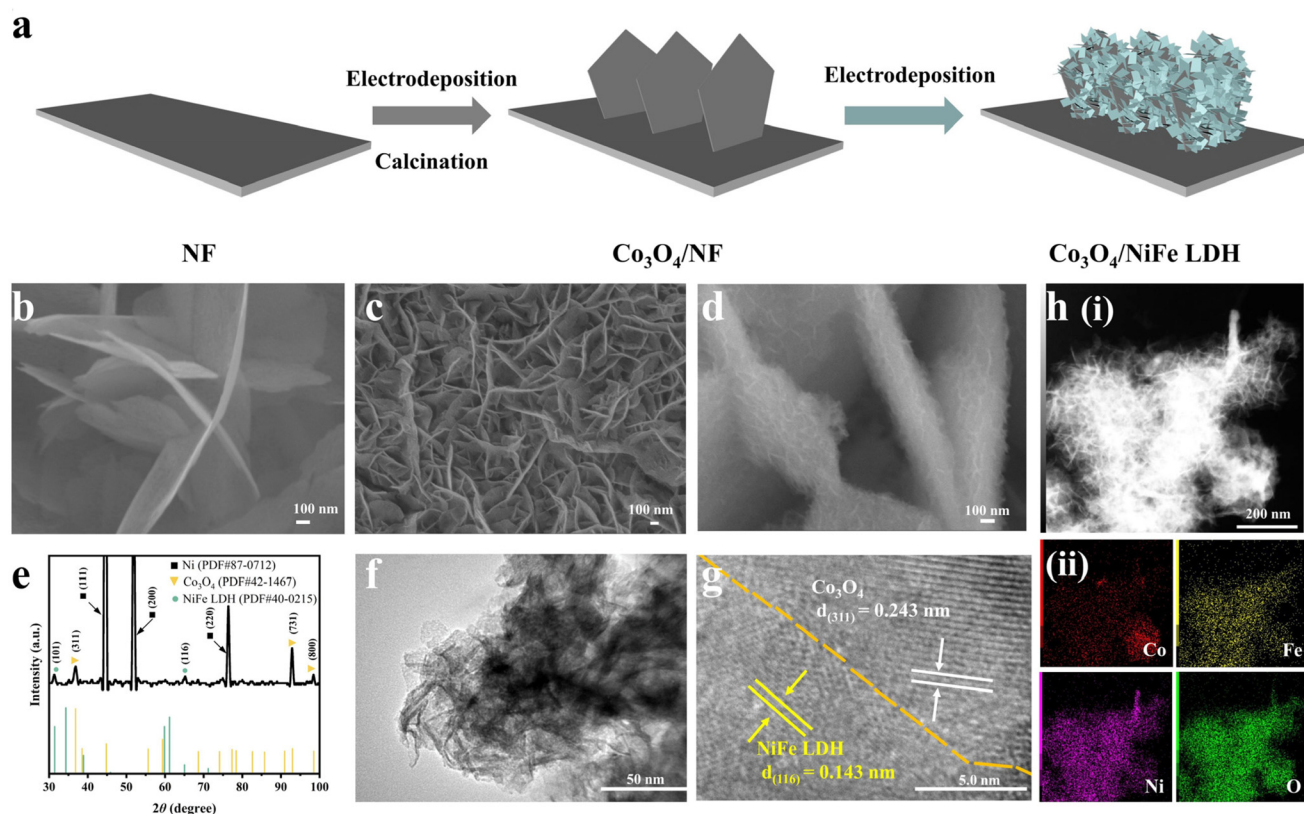**Fig. 1** (a) Illustration of the Co_3O_4/NiFe LDH synthesis. SEM images of (b) Co_3O_4/NF, (c) NiFe LDH/NF and (d) Co_3O_4/NiFe LDH-40. (e) XRD pattern of Co_3O_4/NiFe LDH-40. (f) TEM and (g) HRTEM images of Co_3O_4/NiFe LDH-40. (h) TEM and the corresponding elemental mapping images of Co_3O_4/NiFe LDH-40.

HRTEM image (Fig. 1g), corresponding to the (311) plane of Co_3O_4 and the (116) plane of NiFe LDH, separately, revealing the successful construction of a heterojunction interface constituted by NiFe LDH and Co_3O_4. Elemental mapping images (Fig. 1h) were employed to investigate the distribution of NiFe LDH on the Co_3O_4/NF surface. The distributions of Ni, Fe, Co and O elements are uniform in Fig. 1h, which further confirms the success of Co_3O_4/NiFe LDH-40 synthesis. Furthermore, the selected area electron diffraction (SAED) pattern (Fig. S2†) also provides definite proof of construction of the heterojunction structure. These results suggest that Co_3O_4/NiFe LDH-40 is endowed with a complex interface structure.

X-ray photoelectron spectroscopy (XPS) was utilized to analyze the atomic valence states and surface compositions of catalysts.[28] The survey spectrum (Fig. 2a) was employed to reaffirm the co-existence of the Ni, Fe, Co and O elements in Co_3O_4/NiFe LDH-40. As illustrated in Fig. 2b, the peaks located at 779.3, 780.65, 794.4 and 796.1 eV are present in the high-resolution Co 2p XPS spectrum of Co_3O_4/NiFe LDH-40,[13] which correspond to Co^{3+} $2p^{3/2}$, Co^{2+} $2p^{3/2}$, Co^{3+} $2p^{1/2}$ and Co^{2+} $2p^{1/2}$, respectively. Positive shifts in Co_3O_4/NiFe LDH-40 are observed compared to Co_3O_4/NF, which indicate intense electron interactions between Co_3O_4 and NiFe LDH as well as electron depletion of Co sites. The dominant valence state of Ni in Co_3O_4/NiFe LDH-40 is Ni^{2+}, which is distinctly evidenced by the peaks at 855.6 (Ni^{2+} $2p^{3/2}$) and 873.4 (Ni^{2+} $2p^{1/2}$) eV in Fig. 2c.[29] In addition, the peak at 853.8 eV should be attributed to Ni^0 of the conductive substrate (Ni foam).[30] Notably, Co_3O_4/NiFe LDH-40 in Fig. 2c exhibits distinct negative shifts compared with NiFe LDH/NF, demonstrating the intense electron interactions within Co_3O_4 and NiFe LDH accompanied by the electron-rich structure of Ni sites. Two fitting peaks at 711.8 and 724.9 eV are displayed in the Fe 2p XPS spectrum

(Fig. 2d), corresponding to the Fe^{3+} oxidation state.[31] The peaks show significant positive shifts compared with those of NiFe LDH/NF, which manifests electron depletion of Fe sites when NiFe LDH is coupled with Co_3O_4. The existence of surface adsorbed –OH (M–OH) and lattice oxygen (M–O) in Co_3O_4/NiFe LDH-40 is confirmed by the O 1s spectrum (Fig. S3†), which contains peaks located at 531.4 and 529.6 eV.[32]

Overall, the XPS spectra mentioned above unveil interfacial electronic interactions between Co_3O_4 and NiFe LDH in the heterostructure for optimizing the charge-transfer behavior of metal active sites. After electrodepositing NiFe LDH, the electrons stream from the Fe and Co sites to the Ni site. The electron-deficient Co sites have stronger binding effects with NO_2^-, facilitating the subsequent hydrogenation processes during the NO_2^-RR.[33] Fe ions with a higher valence state can enrich the hydroxyl on the surface of the electrocatalysts to accelerate the OER reaction.[34]

3.2. Electrocatalytic NO_2^-RR and OER performances

The electrocatalytic NO_2^- reduction performance of Co_3O_4/NiFe LDH-40 was investigated in a classical H-type cell containing 35 mL catholyte with 0.1 M NaOH and 0.1 M NO_2^- under an Ar-saturated atmosphere. As illustrated in Fig. 3a and Fig. S6,† the most distinct enhancement of current density belonging to Co_3O_4/NiFe LDH-40 is demonstrated on the linear scanning voltammetry curve in the presence of NO_2^- compared to that without NO_2^-, preliminarily confirming the possibility of high-efficiency reduction of NO_2^- via Co_3O_4/NiFe LDH-40. Chronoamperometric (CA) measurements were conducted on Co_3O_4/NiFe LDH-40 at working voltages ranging from −0.3 to −0.7 V (Fig. S7a†), in order to evaluate in detail the catalytic NH_3 production performance of the electrocatalyst. The indophenol blue photometric method was adopted to analyze the NH_3 produced at various potentials, and the corresponding UV–vis absorption spectrum is shown in Fig. 3b. NH_3 yields and the associated Faraday efficiencies (FEs) of the Co_3O_4/NiFe LDH-40 composite at various potentials are displayed in Fig. 3c. At −0.5 V, Co_3O_4/NiFe LDH-40 simultaneously achieves a maximum NH_3 yield reaching 4.27 mg h^{-1} cm^{-2} and an optimal FE reaching 96.53%. The outstanding NH_3 yield and FE of Co_3O_4/NiFe LDH-40 could also be competitive with those of the various advanced electrocatalysts that have been reported for electrocatalytic NO_2^- reduction (Table S1†). Moreover, the Watt and Chrisp method was employed for the detection of the by-product (N_2H_4) at diverse potentials, and the corresponding results revealing the virtually undetectable N_2H_4 confirm the excellent selectivity of Co_3O_4/NiFe LDH-40 (Fig. S8†).

With a view of demonstrating the significance of the heterostructure formation and the optimized core–shell structure in Co_3O_4/NiFe LDH, in Fig. 3d the contrast in the properties between Co_3O_4/NiFe LDH-40 and related single component materials at the same potential is illustrated. Co_3O_4/NiFe LDH-40 demonstrates superior electrocatalytic activity compared to Co_3O_4/NF (70%, 2 mg h^{-1} cm^{-2}), NiFe LDH/NF (20.3%, 0.8 mg h^{-1} cm^{-2}), and NF (16.8%, 0.5 mg h^{-1} cm^{-2}).
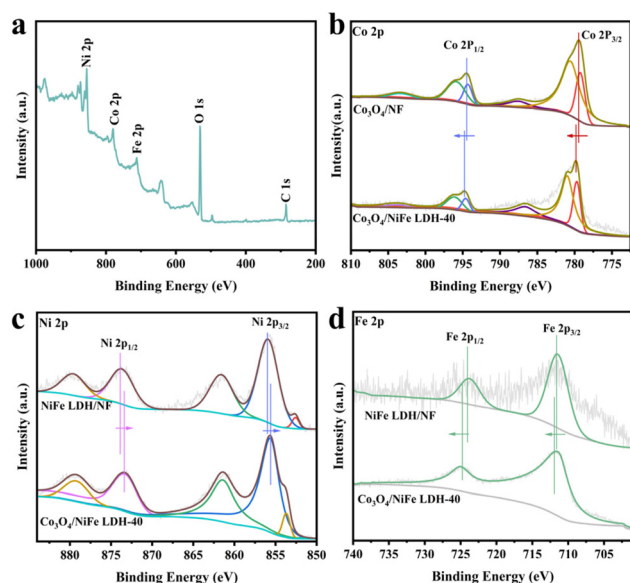

Fig. 2 (a) XPS survey spectrum of Co_3O_4/NiFe LDH-40. (b) Co 2p, (c) Ni 2p and (d) Fe 2p XPS spectra of related materials.
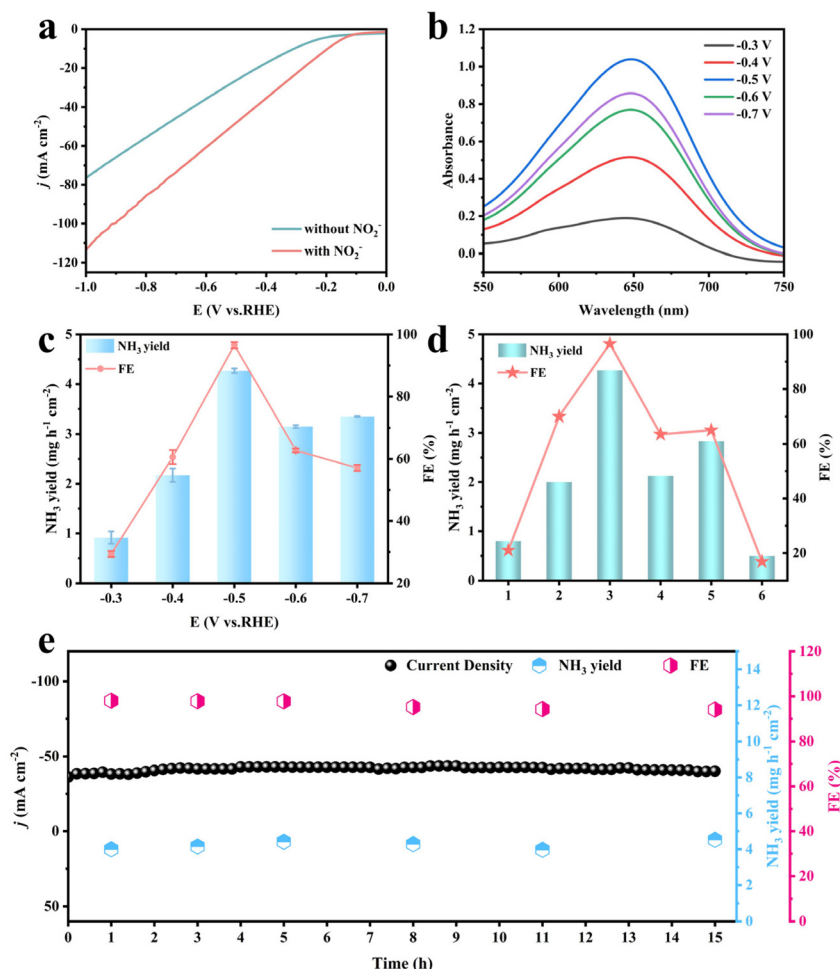
This journal is © the Partner Organisations 2023

Inorg. Chem. Front., 2023, 10, 4510–4518 | 4513

Fig. 3 (a) LSV curves of Co_3O_4/NiFe LDH-40 in 0.1 M NaOH with/without 0.1 M NO_2^-. (b) UV-vis spectra, (c) NH_3 yields and FEs of Co_3O_4/NiFe LDH-40 from −0.3 to −0.7 V. (d) NH_3 yields and FEs belonging to 1. NiFe LDH/NF, 2. Co_3O_4/NF, 3. Co_3O_4/NiFe LDH-40, 4. Co_3O_4/NiFe LDH-20, 5. Co_3O_4/NiFe LDH-60, and 6. NF. (e) Long-term experiment of electrochemical nitrate reduction at −0.5 V and the associated NH_3 yields and FEs.

In detail, the NH_3 yield in Co_3O_4/NiFe LDH-40 is 2.14, 5.31, and 8.62 times higher than that of Co_3O_4/NF, NiFe LDH/NF, and NF, respectively. The distinct difference in the NO_2^-RR performance among Co_3O_4/NiFe LDH-40, Co_3O_4/NF and NiFe LDH/NF reaffirms the favorable contribution of heterostructure construction and core–shell nanostructure design for the NO_2^-RR process.

Co_3O_4/NiFe LDH-40 also exhibits noticeable enhancement in performance compared to Co_3O_4/NiFe LDH-20 and Co_3O_4/NiFe LDH-60, which further confirms the importance of the optimized LDH deposition process for the exposed active area.[35,36] Long-term durability is indisputably a criterion indispensable for assessing the performance of a catalyst,[37–39] and successive electrolysis in Co_3O_4/NiFe LDH-40 was conducted for 15 h at −0.5 V. As depicted in Fig. 3e, the Co_3O_4/NiFe LDH-40 heterostructure maintains relatively stable current density for 15 h at −0.5 V with slight fluctuations in both NH_3 yield and FE, indicating the superior robustness of Co_3O_4/NiFe LDH-40. More intriguingly, scarcely any changes could be noticed in the electronic structure (Fig. S10 and 11†) and mor-

phology (Fig. S12†) of Co_3O_4/NiFe LDH-40 undergoing the 15 h robustness test, further verifying the decent robustness of Co_3O_4/NiFe LDH-40.

The OER properties of related materials were evaluated in 1.0 M KOH. As illustrated in Fig. 4a, Co_3O_4/NiFe LDH-40 simultaneously possesses the most remarkable NO_2^-RR and OER activity. The OER polarization curves (Fig. 4b) demonstrate in detail the optimal OER activity of Co_3O_4/NiFe LDH-40, achieving 100 and 200 mA $cm_{geometric}^{-2}$ with ultralow overpotentials reaching 270 and 300 mV, respectively. Co_3O_4/NiFe LDH-40 simultaneously has the smallest Tafel slope (47.46 mV dec^{-1}) among various electrocatalysts, which also confirms the excellent OER kinetics and the extraordinary charge transfer coefficient of Co_3O_4/NiFe LDH-40. Such an OER performance is intermediate among the Co-based and LDH-based catalysts developed currently (Table S2†), but the activity of Co_3O_4/NiFe LDH-40 is moderately increased compared to that of NiFe LDH and Co_3O_4 synthesized in this work. Moreover, the electrochemical surface area (ECSA) and electrochemical impedance spectra (EIS) were employed to study the remarkable OER per-
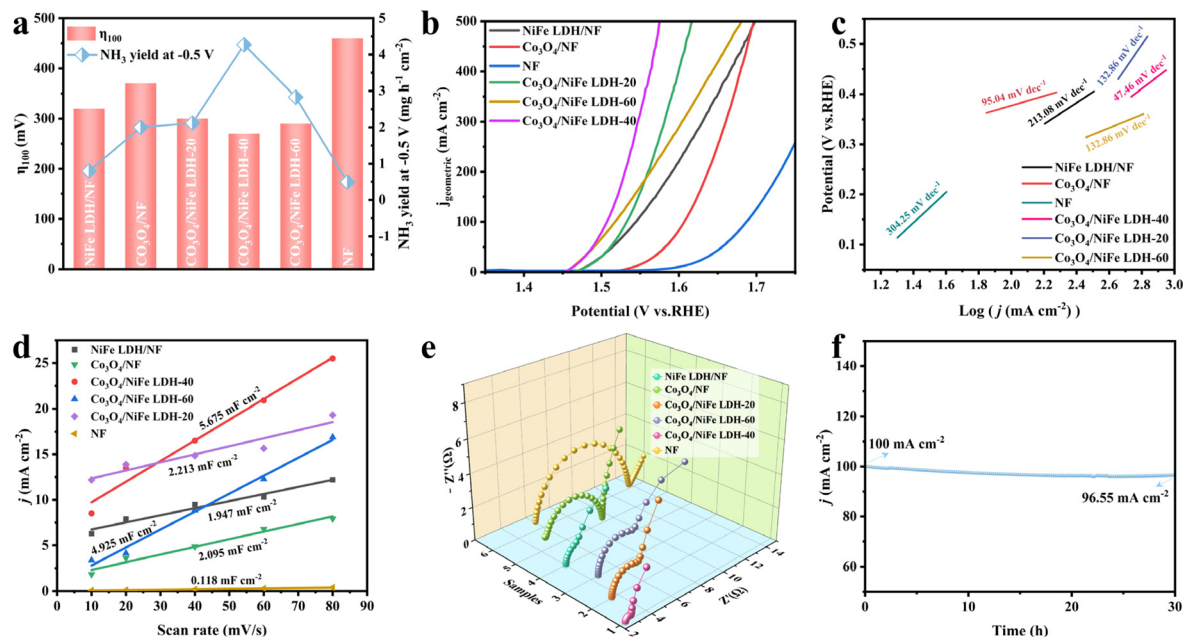
4514 | *Inorg. Chem. Front.*, 2023, **10**, 4510–4518

This journal is © the Partner Organisations 2023

Fig. 4 (a) The comparison of NH_3 yield at -0.5 V and overpotential at 100 mA cm^{-2} of different materials. (b) OER polarization curves based on geometric area, (c) OER Tafel curves, (d) C_{dl} values and (e) Nyquist plots of different electrocatalysts. (f) Chronoamperometric measurements of $Co_3O_4/$NiFe LDH-40.

formance of $Co_3O_4/$NiFe LDH-40. Typically, the ECSA can be derived from double-layer capacitance (C_{dl}, Fig. 4d), which is correlated with the active surface area of electrocatalysts.[12] $Co_3O_4/$NiFe LDH-40 has a larger C_{dl} value (5.675 mF cm^{-2}) than NiFe LDH/NF (1.947 mF cm^{-2}) and $Co_3O_4/$NF (2.095 mF cm^{-2}), confirming that the core–shell structure is conducive to exposing more active sites and enhancing the intrinsic activity of the material. In addition, in order to eliminate the effect of surface area,[40] ECSA normalized LSV curves were also explored for investigating the intrinsic catalytic activity of the catalysts. As illustrated in Fig. S14,† $Co_3O_4/$NiFe LDH-40 still exhibits better OER performance than other contrast electrodes.

Meanwhile, the C_{dl} value of $Co_3O_4/$NiFe LDH-40 is larger than that of $Co_3O_4/$NiFe LDH-20 (2.213 mF cm^{-2}) and $Co_3O_4/$NiFe LDH-60 (4.925 mF cm^{-2}), reaffirming the effect of the NiFe LDH electrodeposition time on the exposure of active sites, which is favorable for maximizing the contact between the catalyst and electrolyte and avoiding the blockage of active sites due to agglomeration. EIS (Fig. 4e) was employed to investigate the charge transfer and mass diffusion processes of the catalysts at the electrode/electrolyte interface. $Co_3O_4/$NiFe LDH-40 exhibits the smallest charge transfer resistance compared to NiFe LDH/NF and $Co_3O_4/$NF, which confirms that the formation of heterogeneous interfaces enhances the electron transfer efficiency and boosts the reaction kinetics for the OER. As for the stability of the electrocatalyst, $Co_3O_4/$NiFe LDH-40 demonstrates outstanding robustness with no significant decay in current density after 30 hours of stability testing (Fig. 4f). The morphology (Fig. S16†) and electronic structure (Fig. S17†) of the material did not display any significant

changes during the long period of the robustness test, reconfirming the promising robustness.

To further confirm the significance of the core–shell structure of $Co_3O_4/$NiFe LDH-40, we prepared non-core–shell $Co_3O_4/$NiFe LDH by changing the time and voltage of NiFe LDH electrodeposition. As depicted in Fig. S18a,† the NiFe LDH nanosheets no longer grow uniformly on the Co_3O_4 nanosheets, but grow interleaved with the Co_3O_4 nanosheets. The non-core–shell $Co_3O_4/$NiFe LDH exhibits worse NO_2^-RR and OER properties (Fig. S18g and h†), and the unsatisfactory stability is verified by the morphology with rapid collapse and agglomeration after the NO_2^-RR and OER (Fig. S18b and c†). The remarkable difference between $Co_3O_4/$NiFe LDH-40 and non-core–shell $Co_3O_4/$NiFe LDH may be derived from the structure. The core–shell structure with Co_3O_4 as the core may prevent the contact between part of Co_3O_4 nanosheets and the electrolyte, resulting in a limited improvement of NO_2^-RR performance. However, the NiFe LDH shell also effectively protects the Co_3O_4 nanosheets thereby achieving more sustained NH_3 production. In addition, the tight coupling between NiFe LDH and Co_3O_4 in the core–shell structure is more beneficial for regulating the electronic structure of Co_3O_4 and accelerating electron transfer than the loose coupling in the non-core–shell $Co_3O_4/$NiFe LDH.

Overall, $Co_3O_4/$NiFe LDH-40 is an NO_2^-RR and OER bifunctional catalyst with low overpotential and superior selectivity. The decent NO_2^-RR and OER bifunctional properties of $Co_3O_4/$NiFe LDH-40 are primarily attributed to two factors: (1) the formation of the heterogeneous structure optimizes the local electronic structure of the active sites, and the electron-
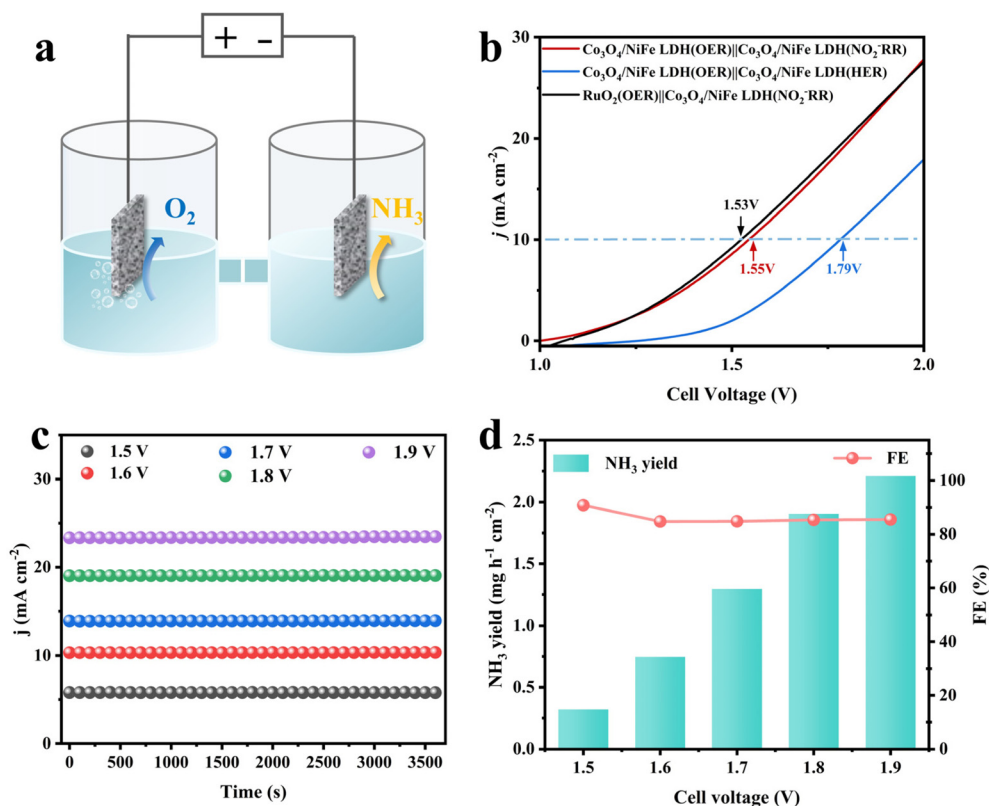
This journal is © the Partner Organisations 2023

Inorg. Chem. Front., 2023, **10**, 4510–4518 | **4515**

Fig. 5 (a) Illustration of the two-electrode OER||NO_2^-RR electrolyzer. (b) LSV curves of relevant two-electrode systems. (c) Chronoamperometry curves, (d) NH_3 yield rate and FE of Co_3O_4/NiFe LDH-40 in the OER||NO_2^-RR system at various applied cell voltages.

deficient Co sites promote the enhanced adsorption of NO_2^- leading to weakening and activation of the N═O bond during the NO_2^-RR,[33] while Fe ions with a higher valence state accelerate the OER and facilitate the release of O_2 from the catalyst surface.[34] (2) The construction of the core–shell structure establishes abundant electrolyte permeation channels and broadens the contact area between the electrocatalyst and electrolyte, which is favorable for obtaining an increased electrochemically active surface area and expedited mass transport.[30]

3.3. Electrocatalytic performance of the NO_2^-RR||OER system

In view of the prominent NO_2^-RR and OER bifunctional activity of Co_3O_4/NiFe LDH-40, it was directly employed as both the anode and cathode of a two-electrode device for ammonia production (Fig. 5a). For comparison, an electrolyzer was also assembled by replacing the anode with advanced RuO_2 having the same load (2.0 mg cm^{-2}) as Co_3O_4/NiFe LDH-40. As shown in Fig. 5b, the Co_3O_4/NiFe LDH-40||Co_3O_4/NiFe LDH-40-assembled electrolytic cell only requires 1.55 V to achieve 10 mA cm^{-2}, which is approaching that of the advanced electrolyzer RuO_2||Co_3O_4/NiFe LDH-40 (1.53 V), confirming the superior OER activity of Co_3O_4/NiFe LDH-40. Intriguingly, the electrolyzer with the cathode reaction supplanted by the HER requires 1.79 V to achieve 10 mA cm^{-2}, significantly exceeding the 1.55 V of the OER||NO_2^-RR system,

demonstrating the inhibitory effect of Co_3O_4/NiFe LDH-40 on the HER. In the Co_3O_4/NiFe LDH-40||Co_3O_4/NiFe LDH-40-assembled electrolytic equipment for ammonia production, the current densities and cathodic NH_3 yields exhibit an increasing trend with rising voltage (Fig. 5c and d). Notably, the faradaic efficiencies of NH_3 remain above 85% under the broad imposed voltage range (1.5–1.9 V), suggesting that the competition of the HER could be effectively inhibited by the approach. The excellent robustness of the electrolyzer assembled with the Co_3O_4/NiFe LDH-40 catalyst is demonstrated by long-term electrolysis (Fig. S19†).

4.   Conclusions

In conclusion, the core–shell Co_3O_4/NiFe LDH heterostructures have been developed to serve as remarkable NO_2^-RR and OER bifunctional electrocatalysts. Benefiting from the optimized electronic structure due to the heterojunction formation and the increased electrochemically active area owing to the core–shell structure construction, Co_3O_4/NiFe LDH exhibits a highly selective and active NO_2^-RR and OER bifunctional performance. The Co_3O_4/NiFe LDH||Co_3O_4/NiFe LDH-assembled electrolytic cell only requires 1.55 V to deliver 10 mA cm^{-2}, which is comparable to that of the electrolyzer assembled with an advanced noble-metal-based catalyst. This effort not only opens up new approaches to explore efficient catalysts *via* regu-

4516 | *Inorg. Chem. Front.*, 2023, **10**, 4510–4518

This journal is © the Partner Organisations 2023

lating interfacial electronic interactions but also offers new insights into achieving high-efficiency and low-cost electrocatalytic ammonia production.

Conflicts of interest

There are no conflicts of interest to declare.

Acknowledgements

References

1 Y. Wang, C. Wang, M. Li, Y. Yu and B. Zhang, Nitrate electroreduction: mechanism insight, in situ characterization, performance evaluation, and challenges, *Chem. Soc. Rev.*, 2021, **50**, 6720–6733, DOI: **10.1039/d1cs00116g**.

2 R. Zhang, S. Zhang, Y. Guo, C. Li, J. Liu, Z. Huang, Y. Zhao, Y. Li and C. Zhi, A Zn-nitrite battery as an energy-output electrocatalytic system for high-efficiency ammonia synthesis using carbon-doped cobalt oxide nanotubes, *Energy Environ. Sci.*, 2022, **15**, 3024–3032, DOI: **10.1039/d2ee00686c**.

3 X. Fan, X. He, X. Ji, L. Zhang, J. Li, L. Hu, X. Li, S. Sun, D. Zheng, Y. Luo, Y. Wang, L. Xie, Q. Liu, B. Ying and X. Sun, High-efficiency electrosynthesis of ammonia with selective reduction of nitrite over an Ag nanoparticle-decorated TiO2 nanoribbon array, *Inorg. Chem. Front.*, 2023, **10**, 1431–1435, DOI: **10.1039/d2qi02409h**.

4 B. Min, Q. Gao, Z. Yan, X. Han, K. Hosmer, A. Campbell and H. Zhu, Powering the Remediation of the Nitrogen Cycle: Progress and Perspectives of Electrochemical Nitrate Reduction, *Ind. Eng. Chem. Res.*, 2021, **60**, 14635–14650, DOI: **10.1021/acs.iecr.1c03072**.

5 K. Fan, W. Xie, J. Li, Y. Sun, P. Xu, Y. Tang, Z. Li and M. Shao, Active hydrogen boosts electrochemical nitrate reduction to ammonia, *Nat. Commun.*, 2022, **13**, 7958, DOI: **10.1038/s41467-022-35664-w**.

6 H. Zhang, G. Wang, C. Wang, Y. Liu, Y. Yang, C. Wang, W. Jiang, L. Fu and J. Xu, CoP nanowires on carbon cloth for electrocatalytic NOx− reduction to ammonia, *J. Electroanal. Chem.*, 2022, **910**, 116171, DOI: **10.1016/j.jelechem.2022.116171**.

7 W. Tian, Y. Ying, J. Ren and Z. Yuan, A trifunctional Co0.85Se/NC collaborated electrocatalyst enables a self-powered energy system for uninterrupted H2 production, *J. Mater. Chem. A*, 2023, **11**, 8024–8037, DOI: **10.1039/d3ta00042g**.

8 J. Ren, L. Chen, W. Tian, X. Song, Q. Kong, H. Wang and Z. Yuan, Rational Synthesis of Core-Shell-Structured Nickel Sulfide-Based Nanostructures for Efficient Seawater Electrolysis, *Small*, 2023, **17**, 2300194, DOI: **10.1002/smll.202300194**.

9 J. Chen, L. Zhang, J. Li, X. He, Y. Zheng, S. Sun, X. Fang, D. Zheng, Y. Luo, Y. Wang, J. Zhang, L. Xie, Z. Cai, Y. Sun, A. A. Alshehri, Q. Kong, C. Tang and X. Sun, High-efficiency overall alkaline seawater splitting: using a nickel-iron sulfide nanosheet array as a bifunctional electrocatalyst, *J. Mater. Chem. A*, 2023, **11**, 1116–1122, DOI: **10.1039/d2ta08568b**.

10 S. Yeon, S. J. Lee, J. Kim, T. Begildayeva, A. Min, J. Theerthagiri, M. L. A. Kumari, L. M. C. Pinto, H. Kong and M. Y. Choi, Sustainable removal of nitrite waste to value-added ammonia on Cu@Cu2O core–shell nanostructures by pulsed laser technique, *Environ. Res.*, 2022, **215**, 114154, DOI: **10.1016/j.envres.2022.114154**.

11 L. Yi, P. Shao, H. Li, M. Zhang, X. Peng, K. Chen, X. Liu and Z. Wen, Scalable synthesis of MoS2 nanosheets electrocatalyst towards high-efficiency nitrite reduction to ammonia, *J. Power Sources*, 2023, **559**, 232668, DOI: **10.1016/j.jpowsour.2023.232668**.

12 X. Fan, C. Ma, D. Zhao, Z. Deng, L. Zhang, Y. Wang, Y. Luo, D. Zheng, T. Li, J. Zhang, S. Sun, Q. Lu and X. Sun, Unveiling selective nitrate reduction to ammonia with Co3O4 nanosheets/TiO2 nanobelt heterostructure catalyst, *J. Colloid Interface Sci.*, 2023, **630**, 714–720, DOI: **10.1016/j.jcis.2022.10.050**.

13 X. Lv, Y. Liu, R. Hao, W. Tian and Z. Yuan, Urchin-like Al-Doped Co3O4 Nanospheres Rich in Surface Oxygen Vacancies Enable Efficient Ammonia Electrosynthesis, *ACS Appl. Mater. Interfaces*, 2020, **12**, 17502–17508, DOI: **10.1021/acsami.0c00647**.

14 Z. Li, J. Liang, Q. Liu, L. Xie, L. Zhang, Y. Ren, L. Yue, N. Li, B. Tang, A. A. Alshehri, M. S. Hamdy, Y. Luo, Q. Kong and X. Sun, High-efficiency ammonia electrosynthesis via selective reduction of nitrate on ZnCo2O4 nanosheet array, *Mater. Today Phys.*, 2022, **23**, 100619, DOI: **10.1016/j.mtphys.2022.100619**.

15 B. Zhang, J. Shan, W. Wang, P. Tsiakaras and Y. Li, Oxygen Vacancy and Core–Shell Heterojunction Engineering of Anemone-Like CoP@CoOOH Bifunctional Electrocatalyst for Efficient Overall Water Splitting, *Small*, 2022, **18**, 2106012, DOI: **10.1002/smll.202106012**.

16 Y. Feng, L. Chen and Z. Yuan, Recent advances in transition metal layered double hydroxide based materials as efficient electrocatalysts, *J. Ind. Eng. Chem.*, 2023, **120**, 27–46, DOI: **10.1016/j.jiec.2022.12.030**.

17 R. Zhao, Q. Li, X. Jiang, S. Huang, G. Fu and J. Lee, Interface engineering in transition metal-based heterostructures for oxygen electrocatalysis, *Mater. Chem. Front.*, 2021, **5**, 1033–1059, DOI: **10.1039/d0qm00729c**.

18 A. Wu, Y. Gu, Y. Xie, H. Yan, Y. Jiao, D. Wang and C. Tian, Interfacial engineering of MoS2/MoN heterostructures as efficient electrocatalyst for pH-universal hydrogen evolution reaction, *J. Alloys Compd.*, 2021, **867**, 159066, DOI: **10.1016/j.jallcom.2021.159066**.

19 X. Li, L. Zheng, S. Liu, T. Ouyang, S. Ye and Z. Liu, Heterostructures of NiFe LDH hierarchically assembled on MoS2 nanosheets as high-efficiency electrocatalysts for

overall water splitting, *Chin. Chem. Lett.*, 2022, **33**, 4761–4765, DOI: 10.1016/j.cclet.2021.12.095.

20 Y. Cao, T. Wang, X. Li, L. Zhang, Y. Luo, F. Zhang, A. M. Asiri, J. Hu, Q. Liu and X. Sun, A hierarchical CuO@NiCo layered double hydroxide core–shell nanoarray as an efficient electrocatalyst for the oxygen evolution reaction, *Inorg. Chem. Front.*, 2021, **8**, 3049–3054, DOI: 10.1039/d1qi00124h.

21 L. Zhang, L. Li, J. Liang, X. Fan, X. He, J. Chen, J. Li, Z. Li, Z. Cai, S. Sun, D. Zheng, Y. Luo, H. Yan, Q. Liu, A. A. Alshehri, X. Guo, X. Sun and B. Ying, Highly efficient and stable oxygen evolution from seawater enabled by a hierarchical NiMoSx microcolumn@NiFe-layered double hydroxide nanosheet array, *Inorg. Chem. Front.*, 2023, **10**, 2766–2775, DOI: 10.1039/d3qi00341h.

22 L. Zhang, J. Liang, L. Yue, K. Dong, J. Li, D. Zhao, Z. Li, S. Sun, Y. Luo, Q. Liu, G. Cui, A. Ali Alshehri, X. Guo and X. Sun, Benzoate anions-intercalated NiFe-layered double hydroxide nanosheet array with enhanced stability for electrochemical seawater oxidation, *Nano Res. Energy*, 2022, **1**, e9120028, DOI: 10.26599/nre.2022.9120028.

23 Q. Mou, Z. Xu, G. Wang, E. Li, J. Liu, P. Zhao, X. Liu, H. Li and G. Cheng, A bimetal hierarchical layer structure MOF grown on Ni foam as a bifunctional catalyst for the OER and HER, *Inorg. Chem. Front.*, 2021, **8**, 2889–2899, DOI: 10.1039/d1qi00267h.

24 C. C. Yang, S. F. Zai, Y. T. Zhou, L. Du and Q. Jiang, Fe3C-Co Nanoparticles Encapsulated in a Hierarchical Structure of N-Doped Carbon as a Multifunctional Electrocatalyst for ORR, OER, and HER, *Adv. Funct. Mater.*, 2019, **29**, 1901949, DOI: 10.1002/adfm.201901949.

25 C. Zhou, E. Hu, S. Liu, W. Cao, Y. Zhu, H. Zhang, T. Zhu, X. Gao and Z. Lin, Boosting oxygen evolution reaction activity and durability of phosphate doped Ni(OH)2/FeOOH hierarchical microtubes by morphology engineering and reconstruction strategy, *J. Colloid Interface Sci.*, 2022, **622**, 319–326, DOI: 10.1016/j.jcis.2022.04.123.

26 X. Guo, X. Hu, D. Wu, C. Jing, W. Liu, Z. Ren, Q. Zhao, X. Jiang, C. Xu, Y. Zhang and N. Hu, Tuning the Bifunctional Oxygen Electrocatalytic Properties of Core–Shell Co3O4@NiFe LDH Catalysts for Zn–Air Batteries: Effects of Interfacial Cation Valences, *ACS Appl. Mater. Interfaces*, 2019, **11**, 21506–21514, DOI: 10.1021/acsami.9b04217.

27 Y. Feng, X. Jiang, L. Tang, D. Lin, Y. Huo, F. Xie and Q. Zheng, Mn-Doped NiFe Layered Double Hydroxide Nanosheets Decorated by Co(OH)2 Nanosheets: A 3-Dimensional Core–Shell Catalyst for Efficient Oxygen Evolution Reaction, *Catal. Lett.*, 2022, **152**, 1719–1728, DOI: 10.1007/s10562-021-03766-7.

28 L. Chen, X. Song, J. Ren and Z. Yuan, Precisely modifying Co2P/black TiO2 S-scheme heterojunction by in situ formed P and C dopants for enhanced photocatalytic H2 production, *Appl. Catal., B*, 2022, **315**, 121546, DOI: 10.1016/j.apcatb.2022.121546.

29 X. Li, Y. Liu, Q. Sun, Z. Huangfu, W. Huang, Z. Wang, C. Chueh, C. Chen and Z. Zhu, Effects of Cationic and Anionic Defects on NiFe LDH in Electrocatalytic Oxygen Evolution, *ACS Sustainable Chem. Eng.*, 2022, **10**, 14474–14485, DOI: 10.1021/acssuschemeng.2c03887.

30 L. Hu, X. Zeng, X. Wei, H. Wang, Y. Wu, W. Gu, L. Shi and C. Zhu, Interface engineering for enhancing electrocatalytic oxygen evolution of NiFe LDH/NiTe heterostructures, *Appl. Catal., B*, 2020, **273**, 119014, DOI: 10.1016/j.apcatb.2020.119014.

31 S. Dutta, A. Indra, Y. Feng, T. Song and U. Paik, Self-Supported Nickel Iron Layered Double Hydroxide-Nickel Selenide Electrocatalyst for Superior Water Splitting Activity, *ACS Appl. Mater. Interfaces*, 2017, **9**, 33766–33774, DOI: 10.1021/acsami.7b07984.

32 Z. Wu, Z. Zou, J. Huang and F. Gao, NiFe2O4 Nanoparticles/NiFe Layered Double-Hydroxide Nanosheet Heterostructure Array for Efficient Overall Water Splitting at Large Current Densities, *ACS Appl. Mater. Interfaces*, 2018, **10**, 26283–26292, DOI: 10.1021/acsami.8b07835.

33 Z. Deng, J. Liang, Q. Liu, C. Ma, L. Xie, L. Yue, Y. Ren, T. Li, Y. Luo, N. Li, B. Tang, A. Ali Alshehri, I. Shakir, P. O. Agboola, S. Yan, B. Zheng, J. Du, Q. Kong and X. Sun, High-efficiency ammonia electrosynthesis on self-supported Co2AlO4 nanoarray in neutral media by selective reduction of nitrate, *Chem. Eng. J.*, 2022, **435**, 135104, DOI: 10.1016/j.cej.2022.135104.

34 X. Wang, Y. Tuo, Y. Zhou, D. Wang, S. Wang and J. Zhang, Ta-doping triggered electronic structural engineering and strain effect in NiFe LDH for enhanced water oxidation, *Chem. Eng. J.*, 2021, **403**, 126297, DOI: 10.1016/j.cej.2020.126297.

35 Y. Zhai, X. Ren, Y. Sun, D. Li, B. Wang and S. F. Liu, Synergistic effect of multiple vacancies to induce lattice oxygen redox in NiFe-layered double hydroxide OER catalysts, *Appl. Catal., B*, 2023, **323**, 122091, DOI: 10.1016/j.apcatb.2022.122091.

36 Z. Yang, Y. Lin, F. Jiao, J. Li, J. Wang and Y. Gong, In situ growth of 3D walnut-like nano-architecture Mo-Ni2P@NiFe LDH/NF arrays for synergistically enhanced overall water splitting, *J. Energy Chem.*, 2020, **49**, 189–197, DOI: 10.1016/j.jechem.2020.02.025.

37 Q. Chen, X. An, Q. Liu, X. Wu, L. Xie, J. Zhang, W. Yao, M. S. Hamdy, Q. Kong and X. Sun, Boosting electrochemical nitrite–ammonia conversion properties by a Cu foam@Cu2O catalyst, *Chem. Commun.*, 2022, **58**, 517–520, DOI: 10.1039/d1cc06215h.

38 A. R. Akbashev, Electrocatalysis Goes Nuts, *ACS Catal.*, 2022, **12**, 4296–4301, DOI: 10.1021/acscatal.2c00123.

39 W. Li, Y. Ye, S. Zhang, C. Liang and H. Zhang, A fluidized electrocatalysis approach for ammonia synthesis using oxygen vacancy-rich Co3O4 nanoparticles, *Inorg. Chem. Front.*, 2021, **8**, 4026–4034, DOI: 10.1039/d1qi00721a.

40 P. Liu, B. Chen, C. Liang, W. Yao, Y. Cui, S. Hu, P. Zou, H. Zhang, H. J. Fan and C. Yang, Tip-Enhanced Electric Field: A New Mechanism Promoting Mass Transfer in Oxygen Evolution Reactions, *Adv. Mater.*, 2021, **33**, 2007377, DOI: 10.1002/adma.202007377.

4518 | *Inorg. Chem. Front.*, 2023, **10**, 4510–4518

This journal is © the Partner Organisations 2023